Martínez-Cisneros, C.S., Ibáñez-García, N., Valdés, F., Alonso, J. (2007). LTCC microflow analyzers with monolithic integration of thermal control. *Sensors and Actuators A: Physical*, 138(1), pp. 63-70.

DOI: 10.1016/j.sna.2007.04.059

LTCC MICROFLOW ANALYZERS WITH MONOLITHIC INTEGRATION OF THERMAL CONTROL

Cynthia S. Martínez-Cisneros[2], Núria Ibáñez-García[1], Francisco Valdés[2], Julián Alonso[1]*

[1]Grup de Sensors i Biosensors. Departament de Química Analítica, Universitat Autònoma de Barcelona, Spain.

[2]Instituto Tecnológico de La Laguna. Torreón, México.

* Author to whom correspondence should be addressed: julian.alonso@uab.es

Tel.: +34935811836, Fax: +34935812379.

ABSTRACT

Recently, the Low Temperature Cofired Ceramics (LTCC) technology has shown to be an excellent alternative to silicon-based microfabrication techniques for the production of three-dimensional structures using a multilayer approach. This enables the integration of several unitary operations of a classical analytical process and also the integration of sensors, actuators and electronics in the same substrate. In this work, we show the integration of the actuators and the sensors needed for the control of temperature inside a miniaturized fluidic device. The proposed device presents enough thermal accuracy to be used in chemical systems where temperature control is a crucial factor, such as enzyme reactions or PCR systems.

KEYWORDS: LTCC, electronics, fluidics, temperature control, miniaturization.

INTRODUCTION

Analytical Chemistry has been deeply influenced by progress in science and technology occurring in recent decades. In particular, the concept of integration has had a deep impact in classical analytical systems, where the integrated parts correspond to the different unitary operations of an analytical process [1].

Despite the fact that current Total Analysis Systems (TAS) provide traceability, precision and accuracy, they also show some disadvantages including: low analysis frequency, high reagent and sample consumption, lack of portability, need of expert users, etc. To solve some of these drawbacks, a new generation of chemical analyzers has been developed: the μ-TAS (micro Total Analysis Systems), involving the integration and scaling down of all the unitary operations of the analytical process [2-4]. The miniaturization of analytical systems has grown rapidly in the area of fluidics. However, the achievement of microdevices integrating fluidics and electronics, producing autonomous and miniaturized analyzers, has been a more difficult challenge.

Among all the materials available for microdevices fabrication, silicon has been the most used. However, there is a recent trend of using polymers because of their low cost and interesting applications. The present work focuses on Low Temperature Co-fired Ceramics or LTCC. This material has been widely applied as an electronic substrate [5-7], not only because it is suitable for high volume and low cost circuit fabrication, but also because it is useful for the construction of multi-layer circuits using surface mounting techniques and thick film technologies. The LTCC technology for printed circuit boards combines the dielectric properties of the ceramic layers with embedded tracks made of highly conductive metals, such as silver or gold [8, 9]. Recently, the multi-layer approach has also been applied to build complex three-dimensional microfluidic structures used as platforms for the fabrication of

miniaturized systems for different analytical process. Table 1 shows a classification of some devices built with LTCC technology.

This paper shows that the LTCC is a suitable technology for the construction of the different elements contained in miniaturized analyzers such as chemical modules (fluid management and chemical pretreatment), detection subsystems and/or the electronics needed for control and measurement purposes. Moreover, LTCC provides an excellent substrate for the monolithic integration of the whole elements allowing complex and small three-dimensional continuous flow analytical systems. In previous work, the suitability of this technology for the fabrication of miniaturized flow systems was demonstrated [29, 30].

In the present work, the integration of a temperature control circuit in a flow system will be presented and discussed to show the suitability of the LTCC technology to integrate microfluidics and electronics monolithically. A temperature control circuit is very useful for chemical and biochemical applications. For instance, it could be applied in Polymerase Chain Reaction (PCR) protocols, where temperature has to be controlled in different zones with an accuracy of ±1ºC [31-34]. Moreover, a large number of enzymatic reactions increase their reaction rates at 37ºC and temperatures higher than 45-50ºC can inhibit their catalytic properties so an accurate temperature control can be very useful in applications involving enzymes.

Several heating/cooling mechanisms have been already reported. Some of them include air cycles [31], external Peltier devices [31, 32] and heating components integrated using screen-printing techniques [34]. Thermocouples have been used as temperature sensors placing them directly in contact with the sample or integrated in proximity to an external heating element [32, 34-36].

To attain a real total analysis microsystem, both the sensor and the heating/cooling elements have to be integrated within the flow system. However, miniaturization techniques based on

silicon, glass or polymers may not be versatile enough to integrate the fluidics and the needed electronics. For that reason, the electronic components are normally placed outside the fluidic device.

Some interesting studies about the compatibility and integration of thick-film thermistors and resistors in LTCC have already been done taking advantage of the use of LTCC as an electronic substrate [37-40].

In this paper, the suitability of the LTCC technology to integrate fluidics and electronics using a single substrate is demonstrated by the monolithic integration of planar resistors used as actuators (heat generation) and thermistors used as sensors with the microfluidics involved for an analytical system.

EXPERIMENTAL

The general LTCC fabrication process of a miniaturized device has been described in detail elsewhere [8, 30]. Although the design, construction and evaluation of a thermal cycler using LTCC technology has been previously reported [37], a new approach is assayed in the present work, integrating fluidics and electronics monolithically.

Materials

Green tape ceramics 951AX, the cofireable solderable Ag/Pd conductor paste 6146 and the resistive paste CF021 (100 ohms/sq) supplied by Dupont were used. The thermistor paste used was R131 (1000 ohm/sq) supplied by Heraeus. A stainless steel screen (50 µm depth) was used for the screen-printing of the pastes. The screen-printer used was a DEK 248 (Asflex Internacional, Spain).

The following components were used to characterize the constructed systems: a peristaltic pump (Minipuls 3, Gilson, Wisconsin, US), 1.02 mm internal diameter silicon tubing (ISMATEC, Zürich, Switzerland), 0.8 mm internal diameter Teflon tubing (SCHARLAB, S.L.,

Cambridge, England), a programmable box oven (CARBOLITE CBCWF11/23P16, Afora, Spain) and a thermocouple-based thermometer (Fluke 179 Multimeter).

Thermistors and resistors construction

The ohmic value of planar resistors is determined by its geometry and the properties of the material as shown by equations 1 and 2 [41], where R is the total resistance of the test structure, R_s (in Ω/square) is the resistivity of the material, *l*, *w* and *t* correspond to the length, width and thickness of the test structure, respectively, and ρ is the resistivity of the paste (in Ω·cm).

$$R = R_s \frac{l}{w} \qquad (1)$$

$$R_s = \frac{\rho}{t} \qquad (2)$$

A rectangular geometry was chosen for better power dissipation and to avoid thermistor warming that would introduce errors to the measurement process. Before the thermistor and resistor pastes were printed and integrated in a fluidic device, they had to be built and evaluated separately to optimize their working area. Different sizes were tried to reach a compromise between the best electrical properties and the smallest size. Ten different areas were tested keeping the ratios l=1.3·w, l=1.6·w and l=2.3·w to obtain resistive values of 5.6 kΩ, 6.8 kΩ and 10 kΩ, respectively for thermistors, and values of 56 Ω, 68 Ω and 100 Ω, respectively for resistors.

Figure 1 shows some of the devices built and tested. Before screen-printing, ceramic layers were dried in an oven at 120ºC for 25 minutes as a preconditioning step. Paths and vias were dried at 100ºC for 5 minutes after the deposition of each paste. The lamination and sintering processes used were those previously described [9, 30].

Fluidic microsystem construction

After the thermistors and the resistors were optimized, they were integrated into a microfluidic structure. The first prototype is shown in figure 2.

Although the thermal conductivity of the ceramic layers (3 W/mK) is smaller than the thermal conductivity of other common materials, such as silicon (148 W/mK at 300K), isolation channels were integrated in the design for heat confinement purposes taking in consideration the accurate temperature control needed for the intended applications. Straight channels were placed on the same layer as the flow channel and a zig-zag channel was placed on a layer above it. None of the isolation channels were in direct contact with the flow channel. Water and air at room temperature were introduced through the isolation channels to get the maximum heat confinement, due to their low thermal conductivities of 0.58 W/mK and 0.0264 W/mK, respectively. Heat was generated by the embedded resistor and temperature was measured at the flow outlet by the thermistor.

Figure 3 shows two more prototypes that were designed after the results obtained with the first one, which showed that heat had a radial distribution, and it would be used to a greater advantage using a radial flow channel. Thus, the flow channels were placed concentrically to the resistor. Two types of isolation structures were tested. The first had a spiral shape through which air flowed for heat isolation. The second isolation structure was formed by 45 air-filled pillars embedded in the structure.

In all the constructed prototypes, cables were soldered to the surface conductor pads, connecting the device to the external electronic module.

Experimental manifold

Thermistors are accurate and sensitive temperature sensors. However, they show a non-linear resistance change as temperature changes [42]. Equation 3 illustrates its exponential behavior,

where R_{T0} is the thermistor resistance at reference temperature, β is the thermistor gain, T_i is the thermistor local temperature and T_0 denotes the reference temperature (in Kelvin) [8]:

$$R_{T_i} = R_{T_0} \exp\left[\beta\left(\frac{1}{T_i} - \frac{1}{T_0}\right)\right] \qquad (3)$$

The non-linear response of the thermistor can be corrected using a linearization circuit as shown in figure 4. Using this circuit, a temperature response linear enough is obtained. The value of the linearization resistor (R_F) should be equal to the resistance of the thermistor at the mid-point of the temperature range of interest. This creates a response whose slope is at its steepest at this mid-point temperature. For our application, R_F was selected to be equal to the thermistor value at 25°C. Applying the linearization circuit, a relation between temperature and potential was established, obtaining an accurate temperature sensor.

The electrical pads of the thermistor were isolated and the device was submerged in a water deposit held at a temperature accurately controlled using a thermostat. The resistance variation as a function of temperature was then measured. A virtual instrument was developed using Labview 7.0 (National Instruments, Santa Clara, CA) to characterize several thermistors simultaneously, speeding the characterization process up.

To characterize the screen-printed heating resistors a high power resistor and a variable power supply were connected in series to the planar element. The power resistor was included to limit the current and the variable supply to obtain a heating power *versus* temperature curve. The temperature was recorded on the surface of the heating resistor as a function of the applied heating power using a temperature sensor LM35 (Analog Devices, Inc. Nashua, NH).

The characterization of the thermistor is crucial for the development of a precise temperature control system. Even though the same experimental procedures were followed during the construction of each thermistor, the devices had to be characterized again once embedded in the microfluidic system. In this case, the re-characterization followed the same methodology

previously described for individual devices, but instead of submerging the devices in a water bath with thermostatic control, a temperature programmable oven was used since ceramics show good thermal conductivity and uniform heat distribution.

In the case of the resistor, the applied potential was controlled to ensure that liquid flowing through would be kept at 37 °C with as little power as possible.

Once assembled and re-characterized, the microfluidic device with the best performance was actuated using a digital PID (Proportional + Integral + Derivative) control system. The PID control was implemented using a microcontroller PIC16F877A (Microchip Technologies, Chandler AZ), Labview 7.0 and a personal computer as the user interface. A block diagram of the electronics in the system is shown in figure 5.

The digital PID control was programmed using the microcontroller and optimizing its parameters electronically. The control signal produced by the PID (a pulse width modulated signal, PWM) was amplified and applied to the resistor embedded in the ceramic system to heat the liquids flowing in its proximity. Temperature in the fluid was measured with the thermistor at the outlet channel and then linearized. The signal from the thermistor was conditioned to the input voltage range of the analog to digital converter in the microcontroller (0 V to 5 V) and then feedback to the controller. The feedback signal read by the microcontroller was used to estimate the error and to correct it using the differential equations programmed in the digital PID control. The system took about five minutes to stabilize before reaching the desired final value or set point of 37 °C.

RESULTS AND DISCUSSION

Resistors and thermistors were evaluated individually at first to find the designs that displayed the best performance. Figure 6 shows the characterization curves obtained for some thermistors after linearization. Most of them showed a linear response. Thermistor T6 was selected as the

best temperature sensor for its small dimensions (0.5 x 0.325 cm), stability, high sensitivity and linear response: $T = -32.4 \cdot E + 3.67$, where T is the temperature (in Kelvin) and E the measured potential (in mV). Additionally, it presents one of the highest slopes. Using this equation, the potential changes from the linearization circuit output potential can be translated to a temperature.

Most of the heating resistors (see Figure 7) were capable of reaching temperatures above 100°C, but R9 (0.5 x 0.21 cm) was chosen as it required the lowest heating power (1.06 W) to reach the highest temperature (111°C).

LTCC materials are good thermal conductors and without isolation most of the heat produced by the resistor would be spread out to the surroundings instead of heating the liquid. The first prototype developed as microfluidic system (see figure 2) included channels both for reagents to flow and for heat isolation. As previously described, two types of isolation channels were built and tested, one following a zig-zag path and two straight paths. The zig-zag channel provided better isolation than the straight ones. With this zig-zag isolation configuration temperatures of 44°C, in the case of water flowing into the isolating channel, and 50°C, using air, were reached. In all cases, water was the fluid being heated. When the straight channels were used for heat isolation, temperatures of 36.2 °C, using water, and 42.8 °C, using air, were reached. The highest temperatures were reached with air due to its lower thermal conductivity coefficient (0.0264 W/mK). In all cases temperature measurements were done with the previously characterized thermistors embedded next to the microfluidic channel outlet. A thermocouple-based thermometer was used as backup. The configuration of this microfluidic device presented a non-uniform heat distribution along the fluid channel. A radial distribution of the temperature was observed promoting the design of new devices (see figure 3). Heat isolation was also implemented in the new microfluidic prototypes in the form of spiral channels with air flowing through them and also as small columns containing air trapped

during the sintering process. Figure 8 shows the temperature reached by the fluid when each approach was followed. The best results were obtained with the spiral channels as isolation. Temperatures over 50°C at the flow outlet were measured using the lowest heating power requirements (3.2 W as maximum).

Since the best isolation was attained with the spiral configuration, a third structure with fewer and wider turns was built (see Figure 9). The thermistor within new device was characterized again showing a linear response of $T = -7.55 \cdot E + 2.72$.

The temperature at the liquid outlet was measured at two flow rates, 0.6 ml/min and 1 ml/min to test the capacity of the microsystem to heat the liquid in the flow channel. Figure 10 shows that temperatures above 40°C were attained in both cases but smaller heating power was required for the flow rate of 0.6 ml/min.

The temperature control was built after the characterization of the final microfluidic device. Figure 11 shows the front panel of the virtual instrument developed as the user interface. This virtual instrument was in constant communication with the microcontroller through the RS-232 serial port. PID constants values (Kp, Ki and Kd) were optimized to get the best response. The final goal of this work was to achieve a temperature control unit integrated in a microflow system, which permits the attainment of a certain constant temperature. Once the experimental conditions and the LTCC microsystem were characterized, we tried to reach a constant temperature of 37°C, needed for enzyme reactions. Figure 10, shows that, having applied a modulated heating power with a maximum of 1 W, 5 minutes were necessary to get the system stabilized. A small over impulse of 1.5°C can also be observed. Finally, a value of 37.36±0.07°C (n=10, 95% confidence), at a flow rate of 0.6 ml/min was monitored for 15 minutes.

CONCLUSIONS

In this work two different but compatible features of the LTCC technology have been used: its ability to serve as a substrate for the fabrication of structures for the fluids management and its suitability as a template for electronic circuits. These features were used in the construction of a three-dimensional miniaturized fluidic system and in the integration of electronic measurement and control components. In particular, a temperature control system based on an actuator (resistor) and a sensor (thermistor) has been designed, characterized and integrated to a microflow system using this convenient and fast prototyping technology. The microsystem reached an accurate temperature control of 37.36±0.07°C that is suitable for some biological reactions, such as those involving enzymes. Additionally, these principles could also be adapted for their use in PCR procedures.

REFERENCES

[1] S. Alegret, in: Integrated Analytical Systems; Alegret, S. (ed.); Elsevier, Amsterdam, 2003, 1-36.

[2] D. R. Reyes, D. Iossifidis, P. A. Auroux and A. Manz, Micro total analysis systems. 1. Introduction, theory, and technology, *Anal. Chem.*, 74 (2002) 2623-2636.

[3] P. A. Auroux, D. Iossifidis, D. Reyes and A. Manz, Micro total analysis systems. 2. Analytical standard operations and applications, *Anal. Chem.*, 74 (2002) 2637-2652.

[4] P. Gravesen, J. Branebjerg and O. S. Jensen, Microfluidics - a review, *J. Micromech. Microeng.*, 3 (1993) 168.

[5] K. B. Shim, N. T. Cho and S. W. Lee, Silver diffusion and microstructure in LTCC multilayer couplers for high frequency applications, *J. Mater. Sci.*, 35 (2000) 813-820.

[6] O. Dernovsek, A. Naeini, G. Preu, W. Wersing, M. Eberstein and W. A. Schiller, LTCC glass-ceramic composites for microwave application, *J. European Ceram. Soc.*, 21 (2001) 1693-1697.

[7] Y. Wang, G. Zhang and J. Ma, Research of LTCC/Cu, Ag multilayer substrate in microelectronic packaging, *Mater. Sci. Eng. B-Solid State Mater. Adv. Technol.* 94 (2002) 48-53.

[8] M. R. Gongora-Rubio, P. Espinoza-Vallejos, L. Sola-Laguna and J. J. Santiago-Avilés, Overview of low temperature co-fired ceramics tape technology for meso-system technology (MsST), *Sensors and Actuators A*, 89 (2001) 222-241.

[9] M. Gongora-Rubio, L. M. Solá-Laguna, P. J. Moffett and J. J. Santiago-Avilés, The utilization of low temperature co-fired ceramics (LTCC-ML) technology for meso-scale EMS, a simple thermistor based flow sensor, *Sensors and Actuators A*, 73 (1999) 215-221.

[10] J. Wilde and Y. Q. Lai, Design optimization of an eddy current sensor using the finite-elements method, *Microelectron. Reliab.*, 43 (2003) 345-349.

[11] U. Schmid, A robust flow sensor for high pressure automotive applications, *Sensors and Actuators A*, 97 (2002) 253-263.

[12] H. Teterycz, J. Kita, R. Bauer, L. J. Golonka, B. W. Licznerski, K. Nitsch and K. Wisniewski, New design of an SnO2 gas sensor on low temperature cofiring ceramics, *Sens. Actuators B-Chem*, 47 (1998) 100-103.

[13] T. Pisarkiewicz, A. Sutor, P. Potempa, W. Maziarz, H. Thust and T. Thelemann, Microsensor based on low temperature cofired ceramics and gas-sensitive thin film, *Thin Solid Films*, 436 (2003) 84-89.

[14] M. A. Fonseca, J. M. English, M. von Arx and M.G. Allen, Wireless micromachined ceramic pressure sensor for high-temperature applications, *J. Microelectromech. Syst.*, 11 (2002) 337-343.

[15] Y. H. Park, C. R. Cho, I. T. Kim, M. W. Lee, K. T. Hwang, J. D. Yu, J. D. Mun, S. S. Kong, B. K. Kim, A. N. Sreeram, K. Palit, M. Liberatore, E. Tormey, L. Hozer and A. Prabhu, in: SID (Society for Information Display), 2000, 478.

[16] J. D. Mun, I. T. Kim, C. R. Cho, K. T. Hwang, S. J. Moon, K. H. Boo, G. J. Moon, S. H. Lee, Y. H. Kwon, M. S. Kim, B. J. Koo, J. K. Han, S. S. Kong and J. D. Kim, in: SID (Society for Information Display), 2002, 1064.

[17] H. Jantunen, T. Kangasvieri, J. Vahakangas and S. Leppavuori, Design aspects of microwave components with LTCC technique, *J. European Ceram. Soc.*, 23 (2003) 2541-2548.

[18] S. H. Sim, C. Y. Kang, J. W. Choi, H. W. W. Choi, Y. J. Yoon, S. Y. Yoon and H. J. J. Kim, A compact lumped-element lowpass filter using low temperature cofired ceramic technology, *J. European Ceram. Soc.*, 23 (2003) 2717-2720.

[19] H. H. Bau, J. Zhu, S. Qian and Y. Xiang, A magneto-hydrodynamically controlled fluidic network, *Sens. Actuators B-Chem*, 88 (2003) 207-218.

[20] J. Zhong, M. Yi and H. H. Bau, Magneto hydrodynamic (MHD) pump fabricated with ceramic tapes, *Sensors and Actuators A*, 96 (2002) 59-66.

[21] J. Li and G. K. Ananthasuresh, Three-dimensional low-temperature co-fired ceramic shells for miniature systems applications, *J. Micromech. Microeng.*, 12 (2002) 198-203.

[22] G. Bischoff, H. Thust, T. Thelemann and T. Kirchner, in: International Symposium on Microelectronics, 1999, 636.

[23] C. F. Chou, R. Changrani, P. Roberts, D. Sadler, J. Burdon, F. Zenhausern, S. Lin, A. Mulholland, N. Swami and R. Terbrueggen, A miniaturized cyclic PCR device - modeling and experiments, *Microelectron. Eng.*, 61-62 (2002) 921-925.

[24] C. S. Henry, M. Zhong, S. M. Lunte, M. Kim, H. Bau and J. J. Santiago, Ceramic microchips for capillary electrophoresis-electrochemistry, *Anal. Commun.*, 36 (1999) 305-307.

[25] K. B. Pfeifer and A. N. Rumpf, Measurement of ion swarm distribution functions in miniature low-temperature co-fired ceramic ion mobility spectrometer drift tubes, *Anal. Chem.*, 77 (2005) 5215-5220.

[26] T. Voß, P. Gründler, A. Kirbs and G. U. Flechsig, Temperature pulse voltammetry: hot layer electrodes made by LTCC technology, *Electrochem. Commun.*, 1 (1999) 383-388.

[27] R. Muller, G. Schuster, A. Rose, O. Hohfeld, R. Blechschmidt-Trapp and R. Werthschutzky, Telemetric system for measuring the pressure of the tongue on the palate, *Biomed. Tech.*, 48 (2003) 226-229.

[28] M. R. G. Rubio, M. B. Fontes, Z. M. da Rocha, E. M. Richter and L. Angnes, LTCC manifold for heavy metal detection system in biomedical and environmental fluids, *Sens. Actuators B- Chem.*, 103 (2004) 468-473.

[29] N. Ibañez-Garcia, R.D. Machado Gonçalves, Z. Mendes da Rocha, M.R. Góngora-Rubio, A.C. Seabra and J. Alonso Chamarro, LTCC meso-analytical system for chloride ion determination in drinking waters, *Sens. Actuators B-Chem.*, 118 (2006) 67-72.

[30] N. Ibañez-Garcia, M. B. Mercader, Z. M. da Rocha, C. A. Seabra, M. R. Gongora-Rubio and J. A. Chamarro, Continuous flow analytical microsystems based on low-temperature co-fired ceramic technology. Integrated potentiometric detection based on solvent polymeric ion-selective electrodes, *Anal. Chem.*, 78 (2006) 2985-2992.

[31] C. T. Wittwer and D. J. Garling, Rapid cycle DNA amplification – Time and temperature optimization, *BioTechniques*, 10 (1991) 76-&.

[32] C. T. Wittwer, C. Fillmore and D. J. Garling, Minimizing the time required for DNA amplification by efficient heat-transfer to small samples, *Anal. Biochem.*, 186 (1990) 328-331.

[33] J. Chiou, P. Matsudaira, A. Sonin and D. Ehrlich, A closed cycle capillary polymerase chain reaction machine, *Anal. Chem.*, 73 (2001) 2018-2021.

[34] M. A. Northrup, in Proc. 8th Int. Conf. Solid State Sensors Actuators (Transducers '95), 1995, .764.

[35] A. T. Woolley, D. Hadley, P. Landre, A. J. de Mello, R. A. Mathies and M. A. Northrup,. Functional integration of PCR amplification and capillary electrophoresis in a microfabricated DNA analysis device, *Anal. Chem.*, 68 (1996) 4081-4086.

[36] P. Wilding, A. Shoffner, J. Cheng, G. Hvichia and J. Kricka, Thermal cycling and surface passivation of micromachined devices for PCR, *J. Clinical Chem.*, 41 (1995) 1367-1367.

[37] J. Zhong, M. Yi and H.H. Bau, Thermal cycler fabricated with low temperature co-fired ceramic tapes, in ASME MEMS, 1999, 123.

[38] J. Zhong and H.H. Bau, Thick film thermistors printed on low temperature co-fired ceramic tapes, *Am. Ceram. Soc. Bull.*, 80 (2001) 39-42.

[39] A. Dziedzic, E. Mis, L. Rebenklau, K.U. Wolter, Geometrical and electrical properties of LTCC and thick-film microresistors, *Microelectron. J.*, 22 (2005) 26.

[40] M. Hrovat, D. Belavic, J. Kita, J. Cilensek, L. Golonka, A. Dziedzic, Thick-film temperature sensors on alumina and LTCC substrate, *J. European Ceram. Soc.*, 25 (2005) 3443.

[41] M. Haskard and K. Pitt, Thick-film technology and applications, Electrochemical Publications LTD, Isle of Man, British Isles, 1997

[42] J. Lepkowski, Microchip Application Notes AN685, Microchip Technology Inc., 1999.

FIGURE 1

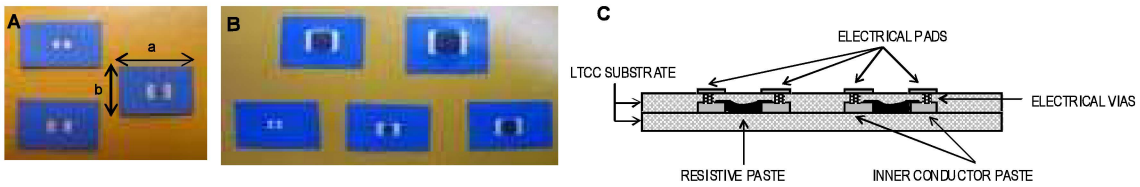
A
a
b
B
C
ELECTRICAL PADS
LTCC SUBSTRATE
ELECTRICAL VIAS
RESISTIVE PASTE
INNER CONDUCTOR PASTE

Figure 2

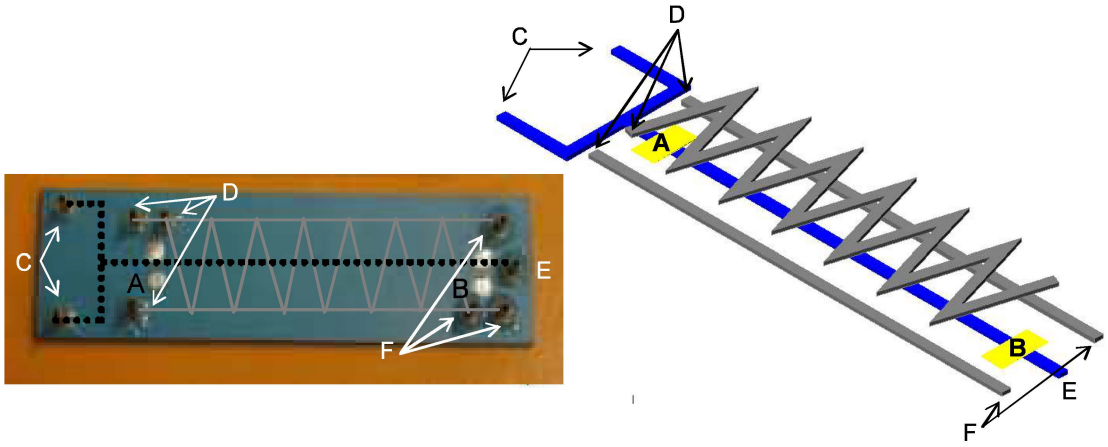

FIGURE 3

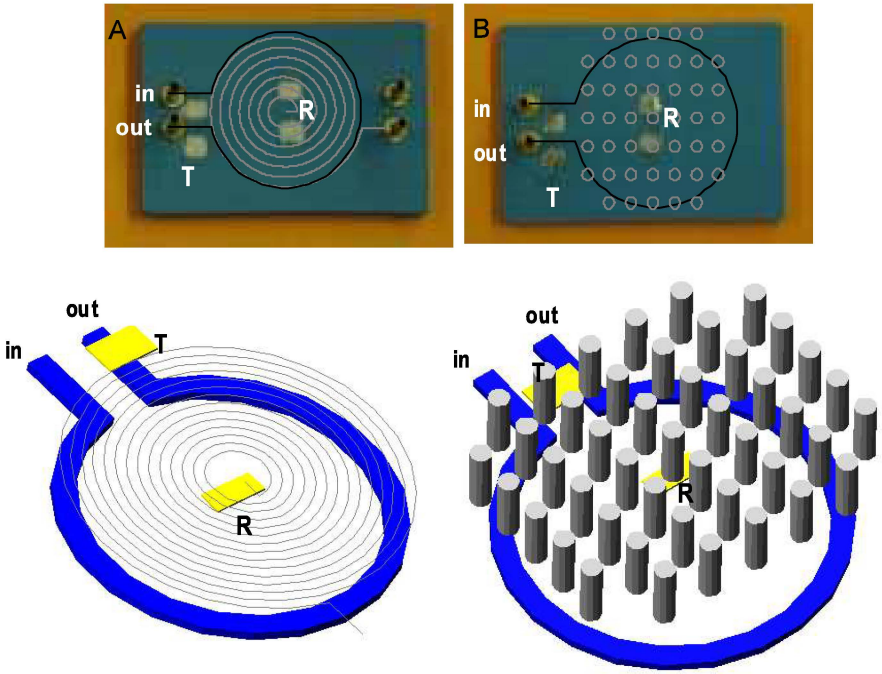

FIGURE 4

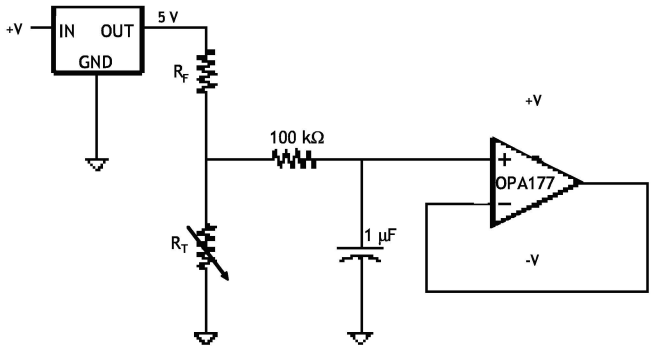

FIGURE 5

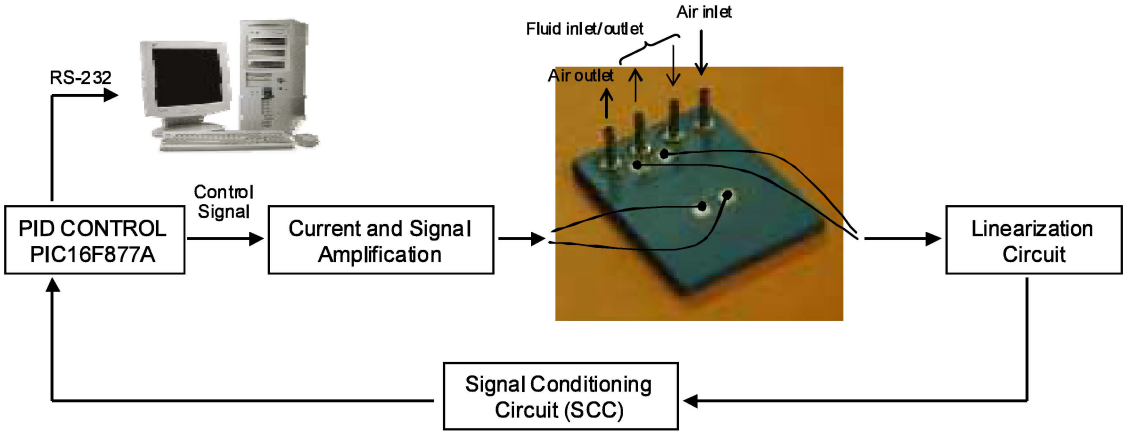
RS-232
Control Signal
PID CONTROL PIC16F877A
Current and Signal Amplification
Fluid inlet/outlet
Air inlet
Air outlet
Linearization Circuit
Signal Conditioning Circuit (SCC)

FIGURE 6

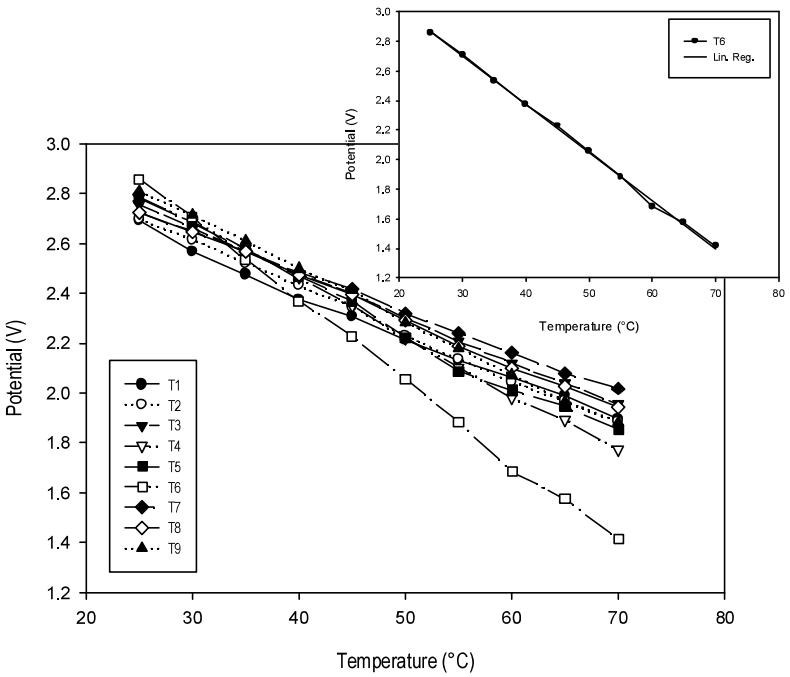

FIGURE 7

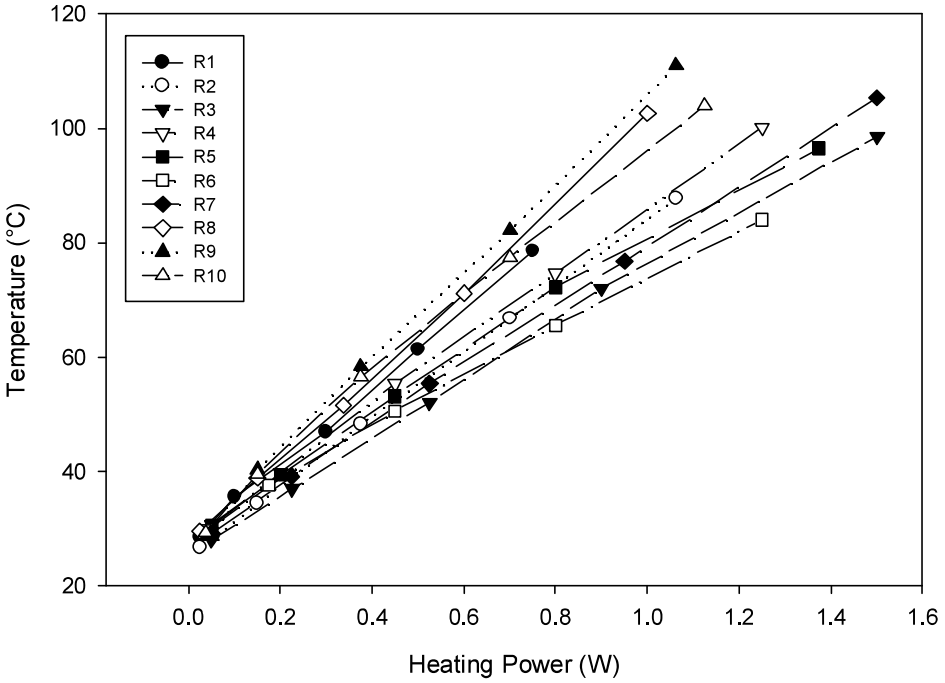
120
100
80
60
40
20
Temperature (°C)
0.0
0.2
0.4
0.6
0.8
1.0
1.2
1.4
1.6
Heating Power (W)
R1
R2
R3
R4
R5
R6
R7
R8
R9
R10

FIGURE 8

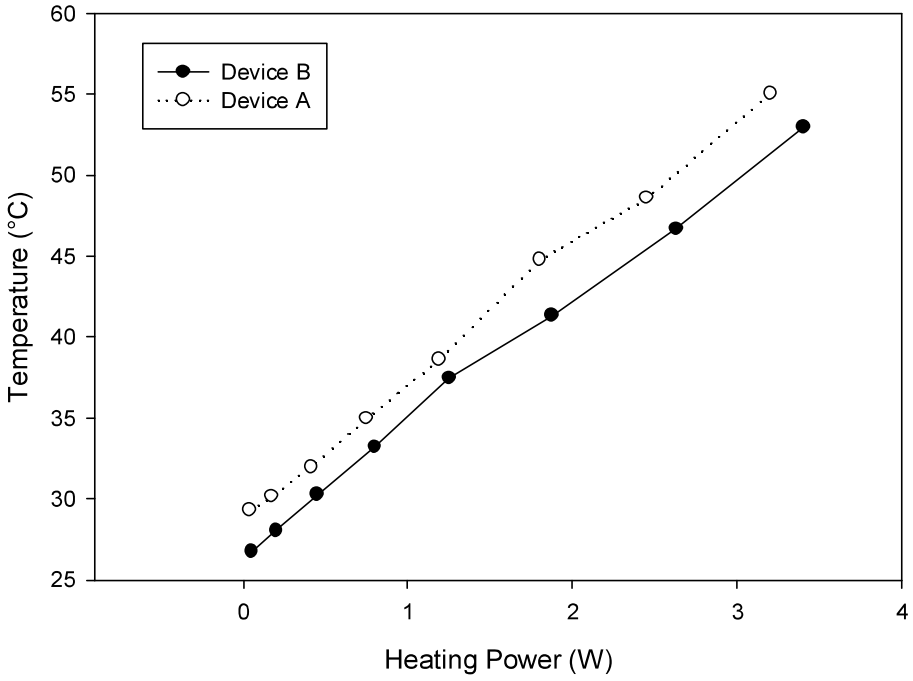
Device B
Device A
Temperature (°C)
Heating Power (W)
60
55
50
45
40
35
30
25
0
1
2
3
4

FIGURE 9

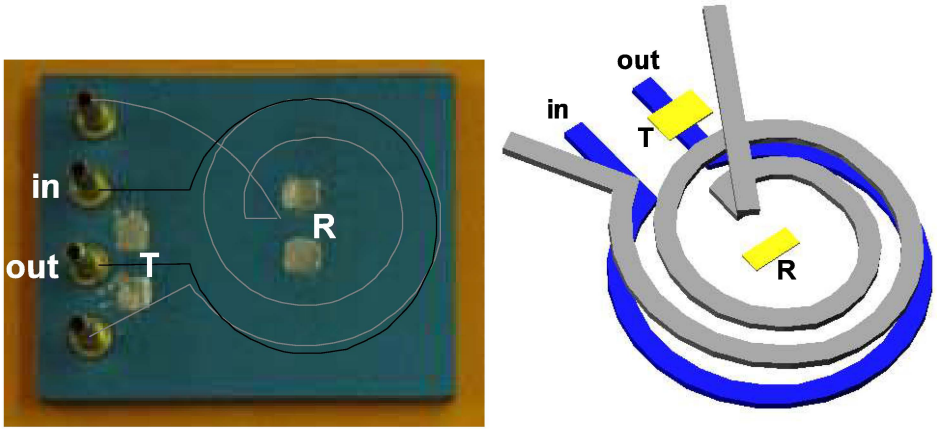

FIGURE 10

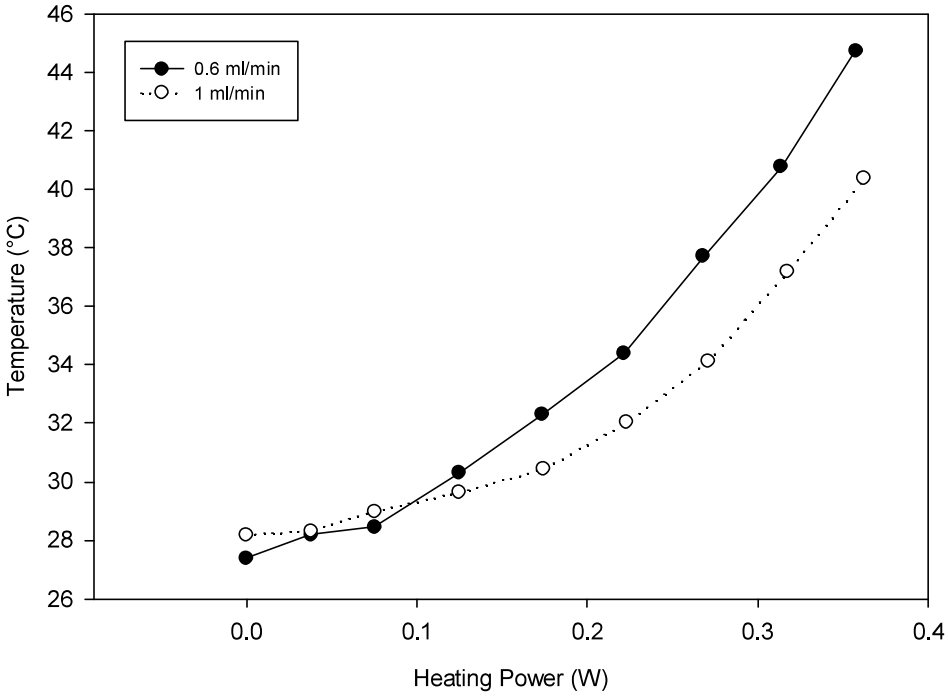
0.6 ml/min
1 ml/min
Temperature (°C)
Heating Power (W)
46
44
42
40
38
36
34
32
30
28
26
0.0
0.1
0.2
0.3
0.4

FIGURE 11

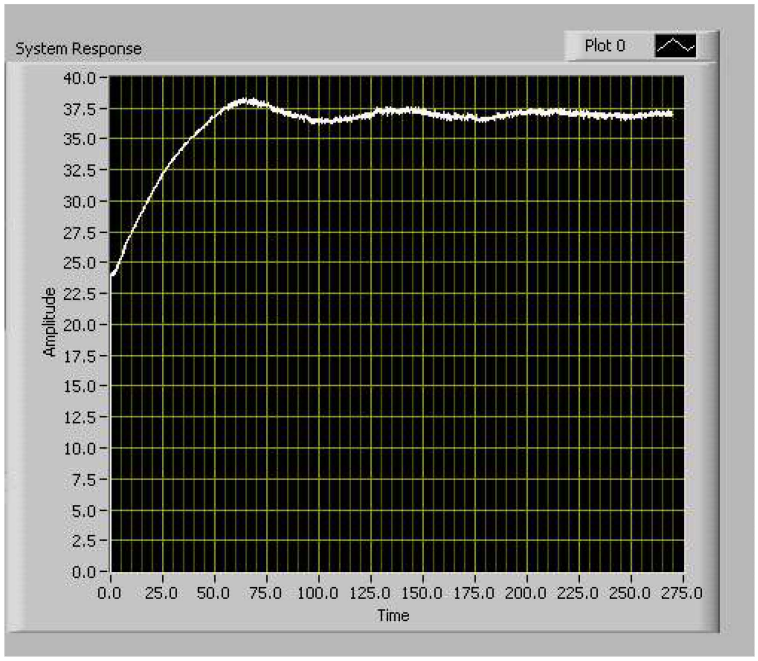
System Response
Plot 0
Amplitude
40.0
37.5
35.0
32.5
30.0
27.5
25.0
22.5
20.0
17.5
15.0
12.5
10.0
7.5
5.0
2.5
0.0
0.0 25.0 50.0 75.0 100.0 125.0 150.0 175.0 200.0 225.0 250.0 275.0
Time

FIGURE CAPTIONS

Figure 1: A: Devices used to evaluate the behavior of the thermistor and the resistor. Connection pads are on their surface. a=1.5 cm, b=1 cm. **B:** Inner conductive areas: black: thermistor, grey: conductors. **C:** Scheme showing where the screen-printing pastes were deposited.

Figure 2: First constructed prototype. In black dots: inner flow channel. In grey lines: heat isolation channels. **A:** embedded resistor. **B:** embedded thermistor. Size: 3x5.4 cm^2. **C:** flow inlets. **D:** isolation channel inlets. **E:** flow outlet. **F:** isolation channel outlets.

Figure 3: Circular prototypes. **A:** Spiral-shape isolation (3x4.6 cm^2). **B:** Pillar-shape isolation (3x4.4 cm^2).

Figure 4: Thermistor linearization circuit. The range of the linear response obtained is around 50°C, where the midpoint is determined by the value of R_F.

Figure 5: Block diagram of the electronics and microfluidics integration. The control signal was generated by a microcontroller and amplified before applying it to the resistor inside the microfluidic system. Temperature measurement was performed by the thermistor at the outlet of the system and used as feedback for the closed loop control system.

Figure 6: **A**. Thermistors characterization curve. Most of thermistors showed a linear response with differences in their slope. **B**. Characterization curve for the thermistor selected for being embedded in the microfluidic device.

Figure 7: Heating resistors characterization. Most resistors reached temperatures around 100 °C varying their current and potential requirements.

Figure 8: Comparative performance of the isolation channels. Higher temperatures were obtained for spiral isolation channels applying the same heating power.

Figure 9: Optimized spiral isolation (3x3.9 cm^2). **In:** flow inlet. **Out:** flow outlet. **R:** resistor. **T:** thermistor.

Figure 10: Temperature reached at two flow rates. Higher temperatures were reached at a flow rate of 0.6 ml/min with less heating power requirements.

Figure 11: A stable response is observed for the PID constants applied to the control system with oscillations of ±0.07 at the stationary stage.

TABLE 1: Applications of the LTCC technology in different areas.

AREA	DEVICE	APPLICATION	REF.
ELECTRONICS	Eddy proximity sensors	Positioning of metallic objects. Mainly applied in the automobilist industry.	10
	Mass flow sensors	Engine control modules (ECM) for fuel injection.	11
	Gas detection sensors	Monitoring of carbon monoxide, ethanol, ozone, hydrogen.	12,13
	Pressure sensors	High temperature pressure sensor in turbine engines.	14
	Plasma Display Panels(PDP)	Reduction of PDP fabrication costs.	15,26
	Radiofrequency and Microwaves	Integration of passive components. Reduction of fabrication costs.	6,17,18
ACTUA-TORS	Micropumps	Flow propulsion to enable, for example, mixing between reagents.	19,20
	Spherical motors	Omni directional wheels.	21
	Passive heating and cooling systems	Generation temperature gradients. Useful for certain biological reactions.	22
CHEMICAL DEVICES	Polymerase Chain Reaction (PCR) devices	DNA identification, genomic cloning, diagnostics.	23
	Electrophoresis	Separation technique.	24
	Ion mobility Spectrometer (IMS) Hot layer electrochemical sensors	Rapid detection of explosive traces and drugs. Studies of proteins denaturalization.	25 26
	Tongue pressure sensors	Control of jaw growth.	27
	Environmental sensors	Monitoring of heavy metals. Monitoring of environmental pollutants in natural and wastewaters: integration of the potentiometric detection system.	28 29,30